Tellus SERIES B CHEMICAL AND PHYSICAL METEOROLOGY
PUBLISHED BY THE INTERNATIONAL METEOROLOGICAL INSTITUTE IN STOCKHOLM

Tellus (2009), 61B, 297–306
Printed in Singapore. All rights reserved

© 2008 Centro de Geofísica de Évora
Journal compilation © 2008 Blackwell Munksgaard

TELLUS

Properties of dust aerosol particles transported to Portugal from the Sahara desert

FRANK WAGNER[1,*], DANIELE BORTOLI[1], SÉRGIO PEREIRA[1], MARIA JOÃO COSTA[1,2], ANA MARIA SILVA[1,2], BERNADETT WEINZIERL[3], MICHAEL ESSELBORN[3], ANDREAS PETZOLD[3], KATHI RASP[3], BERND HEINOLD[4] and INA TEGEN[4], [1]*Centro de Geofísica, Rua Romão Ramalho 59, 7000 Évora, Portugal;* [2]*University of Évora, Physics Department, Rua Romão Ramalho 59, 7000 Évora, Portugal;* [3]*Deutsches Zentrum für Luft- und Raumfahrt, Institut für Physik der Atmosphäre, Oberpfaffenhofen, 82234 Wessling, Germany;* [4]*Leibniz Institute for Tropospheric Research, Leipzig, Germany*

(Manuscript received 7 February 2008; in final form 14 August 2008)

ABSTRACT

Aerosol properties of mineral particles in the far field of an African desert dust outbreak were investigated that brought Saharan dust over the Mediterranean in different layers to Portugal. The measurements were performed inside the project Desert Aerosols over Portugal (DARPO) which was linked to the Saharan Mineral Dust Experiment (SAMUM). The maximum particle mass concentration was about 150 μg m^{-3} and the corresponding scattering coefficient was 130 M m^{-1} which results in a mass scattering efficiency of 0.87 m^2 g^{-1}. The aerosol optical depth reached values up to 0.53 and the lidar ratio was between 45 and 50 in the whole dust loaded column. A comparison between particle size distributions and refractive indices derived from different instruments and models showed a general good agreement but some minor differences could also be observed. Measurements as well as calculations with a particle transport model suggest that there is a relatively higher concentration of very large particles in the upper region of the dust layer than on the surface which is likely connected with meteorological conditions at the observational site (Évora, Portugal).

1. Introduction

Desert dust is one of the major constituents of natural aerosol particles in the atmosphere and the African Sahara is the largest desert area and also the primary dust source on Earth (Washington et al., 2003). Particles originating from there are transported over several thousands of kilometres over the Atlantic Ocean as far as North America (see e.g. Prospero, 1999), and over Europe reaching northern latitudes as far as England, Northern Germany and Denmark (Ansmann et al., 2003). A desert dust outbreak is also one of the main causes, which leads high PM10 particle mass concentrations in Southern Europe (see e.g. Rodríguez et al., 2001; Borge et al., 2007).

Mineral dust particles scatter and absorb radiation. Due to the significant portion of larger particles, desert dust not only influences the short-wave (or solar) radiation but also the long-wave (terrestrial) radiation. In terms of an energy balance the short- and long-wave radiative effects have different signs and therefore they partially cancel out (see e.g. Haywood et al., 2001). At the surface the incoming solar energy is reduced due to scattering and absorption of dust particles. This loss is in part compensated by an increase in long-wave radiation due to emission of radiation by dust (Claquin et al., 1998). The vertical distribution of mineral particles influences the top-of-the-atmosphere radiative flux and hence the radiative forcing both at the top-of-the-atmosphere and at the surface. Moreover atmospheric heating rates are altered (see e.g. Carlson and Benjamin, 1980).

Besides routine measurements in various places on the world several experiments have already been conducted to determine properties and effects of desert dust. Recently the experiments Saharan Dust Experiment (SHADE, 2000, Cape Verde, see e.g. Tanré et al., 2003), Puerto Rico Dust Experiment (PRIDE, 2001, Puerto Rico, see e.g. Reid et al., 2003) and African Monsoon Multidisciplinary Analyses (AMMA, 2006, West Africa, see e.g. Redelsperger et al., 2006) were performed.

The experiment Saharan Mineral Dust Experiment (SAMUM) took place in May/June 2006 in Morocco and aimed at characterizing the properties and assessing the effects of desert dust close to the source regions. At the same time the project Desert Aerosols over Portugal (DARPO) was conducted over

*Corresponding author.
e-mail: frankwagner@uevora.pt
DOI: 10.1111/j.1600-0889.2008.00393.x

continental Portugal and focused on evaluating the properties of desert dust after transportation over long distances (at least 800 km) from Africa to Portugal. During this time a desert dust outbreak occurred, transporting mineral particles from Morocco and Algeria via Spain to Portugal. A flight between Morocco and Portugal was performed with the Falcon aircraft linking source region and far-field region together.

In this work joint in situ and remote sensing measurements as well as a mesoscale model are used to investigate optical and microphysical properties of desert dust particles after transportation to Portugal. Investigations using combined platforms – specifically aiming on mineral dust properties – are rare for the Iberian Peninsula and especially for its western part (Portugal). Cachorro et al. (2006) focused on optical properties of desert dust and additionally reported columnar microphysical properties for southwest Spain. Perez et al. (2006) combined remote sensing measurements with a regional model. Russell and Heintzenberg (2000) as well as Elias et al. (2006) gave an overview over several aerosol types (including desert dust) over Portugal. But they only reported a few optical and none microphysical properties of mineral dust. The present study is indeed the first study in the western part of the Iberian Peninsula where optical and microphysical desert dust aerosol properties are derived from coupling different observational platforms and a mesoscale model.

First, the temporal evolution of several aerosol quantities at Évora, Portugal near the ground is shown and after for the time of the aircraft overpass a comparison of optical particle as well as microphysical properties is done.

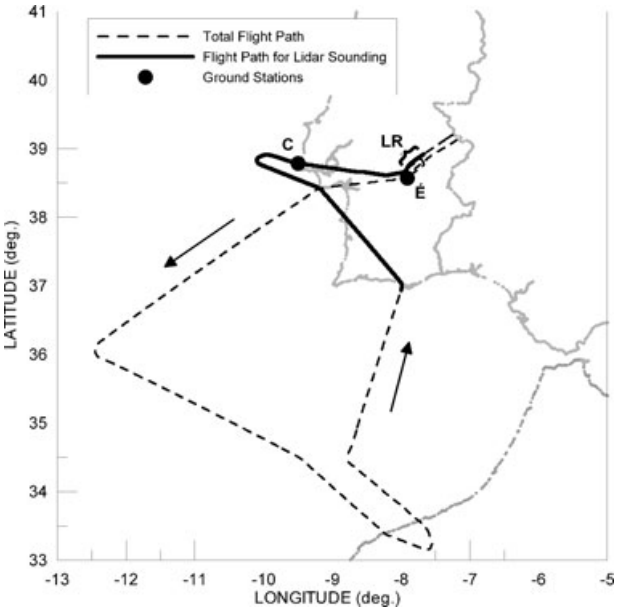

Fig. 1. Map showing the location of the ground stations Évora (É) and Cabo da Roca (C) in Portugal and the whole flight path of the airplane from Morocco to Portugal and back (dotted line). The solid thick line denotes the path for the lidar sounding as shown in Fig. 6, the curly bracket indicates the path which was used to determine the lidar ratio, LR (see Fig. 7) and the arrows indicate the flight direction.

2. Instruments, data and methods

The main observational platform was located at Évora, Portugal (38.57°N, 7.91°W, 293 m asl). There, several ground-based instruments were used to investigate the temporal evolution of the desert dust plume, which arrived in Portugal in the end of May 2006. Additionally on the coast at Cabo da Roca, Portugal (38.78°N, 9.5°W, 140 m asl) a sun photometer was operated. Figure 1 shows the geographic location of the measuring sites.

A tapered element oscillating microbalance (Rupprecht and Patashnik TEOM) was operated continuously with a temporal resolution of 10 min and using a PM10 inlet providing the particle mass concentration. Due to losses of volatile material, the device has to be calibrated. This was done extensively (Pereira, 2006) against a gravimetric high volume sampler (Andersen Samplers, Inc). The local contribution to the particle mass concentration can be estimated by averaging the days with the absence of long-range transported particles. Pereira et al. (2008) showed that the diurnal and weekly cycles of the aerosol mass concentration are mainly caused by urban activities. The obtained results are used for this work.

A nephelometer was continuously operated with a temporal resolution of 5 min and using a PM10 inlet. The instrument is calibrated once a year using dry air and CO_2. The Anderson and Ogren (1998) correction was applied to all measured values to take into account Lambertian and truncation errors of the instrument and to obtain the scattering coefficients at the three wavelengths 450, 550 and 700 nm.

An aerodynamic particle sizer (APS) was measuring without inlet continuously with a temporal resolution of 5 min providing the particle size distribution between roughly 0.5 and 20 μm aerodynamic diameter. Because the APS provides in all cases a particle distribution with respect to the aerodynamic particle diameter, this diameter was transformed into a geometric diameter via $d_{\mathrm{aero}} = \sqrt{\rho} d_{\mathrm{geo}}$ where d_{aero} denotes the aerodynamic diameter, d_{geo} the geometric diameter and ρ stands for the particle density (see Hinds, 1999). We have no knowledge about the actual particle shape. Hence no shape correction was applied. We assumed a mean density of 2.5 g cm^{-3} for desert dust aerosols. We chose this value to be at the lower end of the range of desert dust particle densities reported in the literature (see Table 1 as reference) because it can be expected that, due to ageing processes, the density of mineral particles will decrease.

A sun photometer (Cimel$^{\mathrm{TM}}$) was operated automatically during daytime proving the aerosol optical depth (AOD) at 440, 675, 870 and 1020 nm. It is part of the AERONET network (Holben et al., 1998) and hence calibration and data analysis were done according to AERONET procedures. From Sun and sky

Table 1. Examples of the density of desert dust particles as reported in the literature

Density (g cm^{-3})	Place of observation	Reference
2.6	World	Hess et al. (1998)
2.5	Northern China, Gobi desert	Fratini et al. (2007)
2.71–2.75	Mojave desert	Winfield (2000)
2.65	Laboratory	Fletcher (1976)
2.65	Northwest China	Shen et al. (2005)
2.6	China	Iwasaka et al. (2003) based on Ishizaka and Ono (1982)

brightness measurements the particle size distribution as well as the complex refractive index can be estimated via the inversion procedure developed by Dubovik and King (2000) and further developed by Dubovik et al. The method also includes a spheroid model to account for particle non-sphericity in the presence of desert dust particles (Dubovik et al., 2006). Another sun photometer (Microtops^{TM}) with five channels centred at 340, 440, 500, 870 and 1020 nm is a handheld sun photometer which was calibrated using the Langley plot method. The AODs of both sun photometers were compared regularly and showed a good agreement.

On the 27 May 2006 the aircraft Falcon was flying several lags over Évora at two different altitudes. The aircraft was equipped with various particle in situ measuring instruments from which the aerosol size distribution between 4 nm and 100 μm and a mean refractive index at three wavelengths between 467 and 660 nm could be derived. Details about instrumentation and the respective derived quantities can be found in Weinzierl et al. (2008) and Petzold et al. (2008) and about the retrieval algorithm in Fiebig et al. (2005). Furthermore, onboard the aircraft, a high spectral resolution lidar (HSR lidar) was operated which provided the vertical profile of the particle extinction and backscattering coefficient. Details about the lidar instrument can be found in Esselborn et al. (2008). A comparison between sun photometer and HSR lidar derived AOD showed very good agreement giving confidence in the lidar measurements and retrieval algorithms (Esselborn et al., 2008).

Furthermore, the measurements of particle size distributions as well as from sun photometer measurements retrieved size distributions are compared with results from the regional dust model-system LM-MUSCAT-DES (Heinold et al., 2007). The model consists of the regional meteorological model 'Lokal-Modell' (LM) from the German Weather Service Deutscher Wetterdienst (DWD) and the multiscale chemical aerosol transport model (MUSCAT), including a dust emission scheme (Tegen et al., 2002).

Emission and transport of mineral dust are calculated on the basis of meteorological and hydrological conditions from the meteorological model LM. Dust is transported as passive tracer in five independent size classes with radius limits at 0.1, 0.3, 0.9, 2.6, 8 and 24 μm; distributions of other aerosols are not considered. Simulations were performed for the period from 9 May to 5 June 2006. The model domain (lower left corner: 13.86°N, 25.35°W; upper right corner: 47.78°N, 38.16°W) has a horizontal resolution of 28 km and covers major parts of the Sahara desert and Central Europe ensuring that synoptic and regional scale weather systems as well as local and long-range dust transport are captured. Details can be found in Heinold et al. (2008).

3. Results

In this section, the time-series of several particle properties will be shown for the pre-phase (starting on 26 May 2006) and for the main phase (27–29 May 2006) of the desert dust outbreak. Then, in the second part of this section, a detailed investigation of several particle parameters for the time of the aircraft over flight over Évora (10:30–11:00 on 27 May 2006) will be done. The overpass nearly coincided with the maximum particle mass concentration at the surface.

3.1. Time-series

Figure 2 shows the development of the particle mass concentration at the surface measured at the observational platform of the CGE at Évora, Portugal. Included in the figure are typical background conditions for weekdays and weekend days (see Pereira et al., 2008). Around midnight on the 26 May the particle mass concentration showed nearly background conditions. After noon an increase of the particle mass by a factor of 3 could be observed. This increase is caused by an increase of larger particles (see also the Ångström exponent, AE, in Fig. 3) which were very likely mineral particles originating in the African desert as will be shown later (compare Fig. 5). Then the particle concentration decreased significantly down to the background conditions. This short episode of desert dust particle is called the pre-phase. The main phase of the desert dust arrival at Évora occurred on 27 May 2006 around 6 UTC which is marked by a sharp increase of the particle mass concentration up to 150 μg m^{-3}. This phase lasted until 29 May 2006 during which a mass concentration decrease can be noted. During the main phase, the concentration of dust particles had reached a value which is about a factor of 7 higher than the typical background values (around 20 μgm^{-3}).

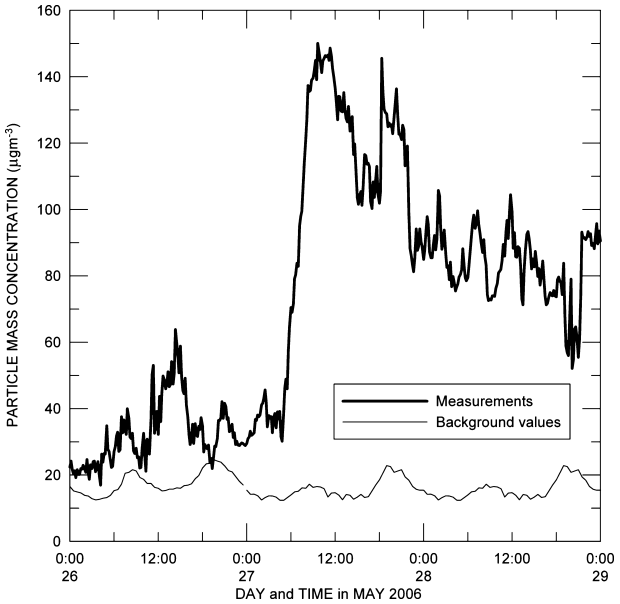

Fig. 2. Particle mass concentration obtained with a TEOM. The thick black curve corresponds to the actual measurements in May 2006 whereas thin black curve describes the background mass concentration as derived in Pereira et al. (2008).

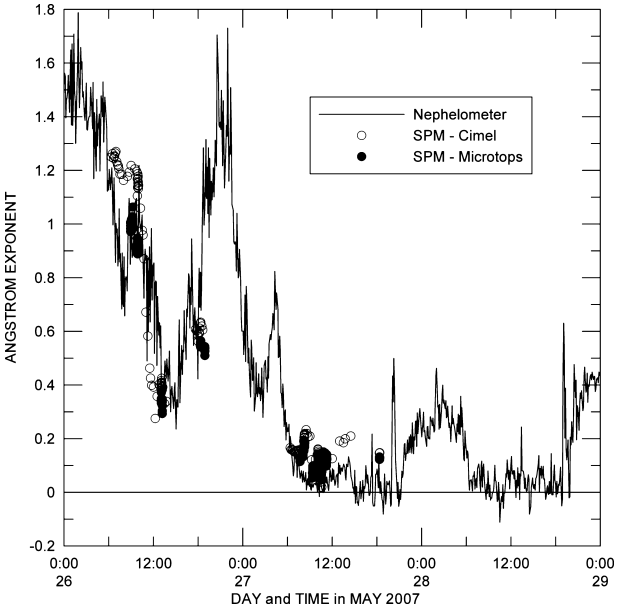

Fig. 3. Ångström exponent determined from nephelometer data (Anderson and Ogren correction applied, 450–700 nm), sun photometer Cimel (AERONET, level 1.5, 440–870 nm) and sun photometer Microtops (440–870 nm).

Figure 3 shows the AE derived from two different sun photometers and the nephelometer. Hereby the wavelength range is similar for all instruments (440–870 nm for the sun photometer and 450–700 nm for the nephelometer). It can be seen that in

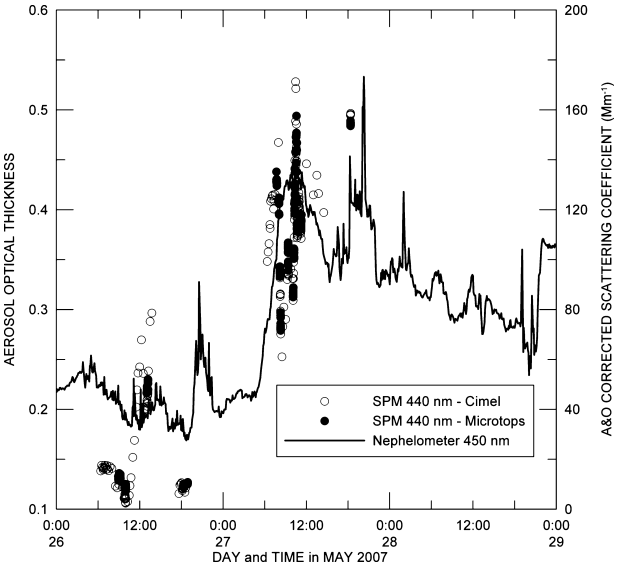

Fig. 4. Aerosol optical thickness at 440 nm retrieved from two different sun photometers and scattering coefficient determined with a nephelometer and corrected for truncation and Lambert error (see Andersen and Ogren 1998).

the pre-phase the AE dropped down to low values of around 0.4 and in the main phase to even lower values of about 0.1. Such low values are characteristic of a relatively high amount of large particles in comparison to the presence of small particles and are typical of desert dust particles. The difference in the AE between pre-phase and main phase can be related to the different influence of locally produced aerosols (more than 50% of PM10 particle mass concentration during the pre-phase compared with less than 25% during the main phase).

Using typical values of the error of the AOD (0.02 for 440 nm, 0.01 for 870 nm, see e.g. Holben et al., 1998; Eck et al., 1999) together with error propagation law gives an error in the AE of less than 0.15. The error for the AE derived from nephelometer cannot be determined, because the applied correction function (Anderson and Ogren, 1998) depends on the actual particle size distribution, which is unknown. However, the effect of the correction function can be assessed by comparing the AEs before and after the correction. The difference in AEs for the desert dust episode was between ± 0.1 and below 0.2 outside. These values might be taken as estimation of the uncertainty in the AE retrievals.

Taking the values provided in Fig. 3 and the respective errors of the AE into account, it can be concluded that the AE derived from all three instruments are in agreement and furthermore that the particle properties near the surface are similar to the ones in the column which is a strong hint that the aerosol type does not change with height.

Figure 4 shows the particle scattering coefficient obtained from nephelometer measurements and the AODs determined from two different sun photometers Cimel and Microtops. The

AOD derived with the Cimel instrument was automatically cloud screened according to AERONET routines (see Smirnov et al., 2000). The other sun photometer (Microtops) is a handheld device and was operated manually. It was only measuring when no clouds were visible in the path between the instrument and the Sun. Hence the cloud screening is intrinsically done during measurement procedure. Note that the different number of measurements between the two sun photometers is rather caused due to the frequency of manual operations and not due to a more or less effective cloud screening procedure.

It is obvious from the figure that the AOD and hence the particle concentration in the atmospheric column vary much more than the scattering coefficient obtained at ground level. This is likely due to particle transport processes above the mixing layer causing horizontal inhomogeneities together with different pointing paths of the sun photometers due to the movement of the Sun.

The relatively high scattering coefficient (Fig. 4) and the relatively low particle mass concentration (Fig. 2) about 9 pm between pre-phase and main phase were caused by local, urban particle production, which is characterized by small particles (high scattering coefficient and low particle mass concentration). At this time desert dust was absent near the ground as can be concluded from the AE value of about 1.6 (Fig. 3).

From the scattering coefficient and the particle mass concentration the mass scattering efficiency of aerosols can be derived. For the main phase of the desert dust outbreak this quantity was about 1 or slightly below 1 $m^2\ g^{-1}$ independently of particle concentration. Such values lie within the range of mass scattering efficiencies reported in the literature (see Hand and Malm, 2007 for a review).

Figure 5a shows 120 h back trajectories arriving at Évora at 3 km altitude. They were calculated with the HYSPLIT model (Draxler and Rolph, 2003; Rolph, 2003). The trajectories

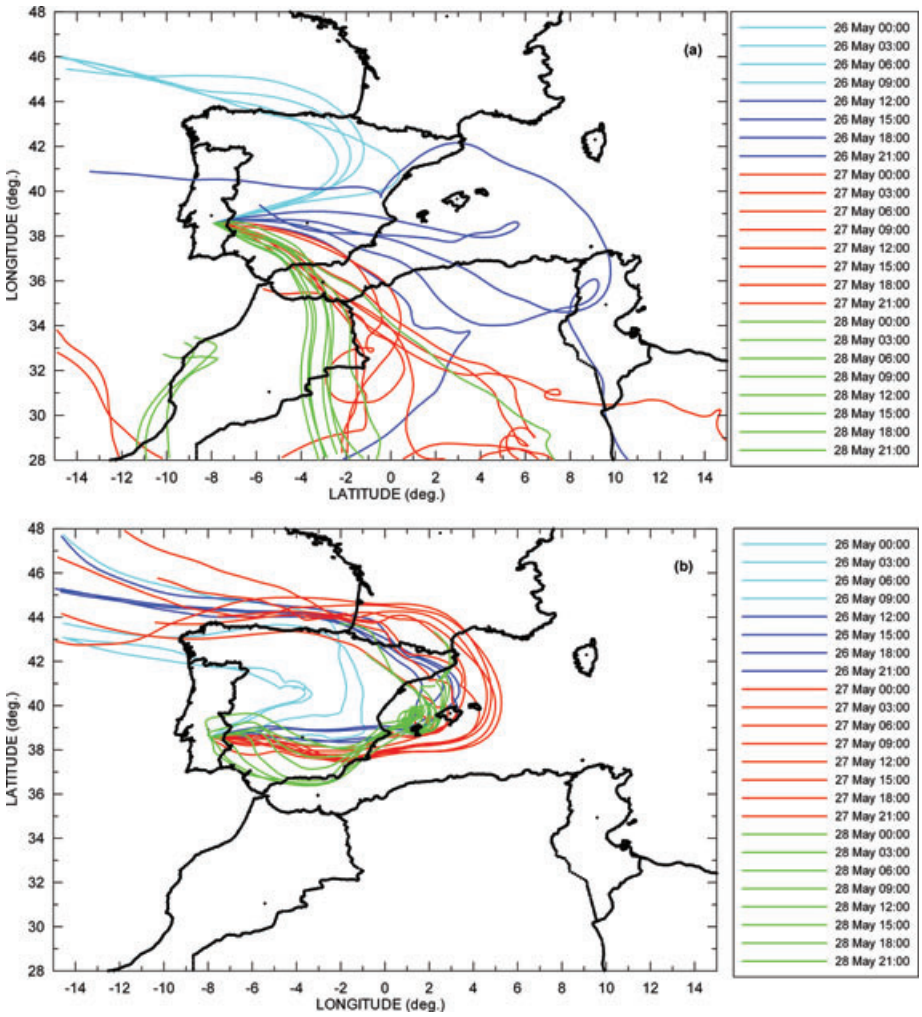

Fig. 5. (a) 120 h-back trajectories arriving at 3000 m asl at Évora, Portugal. (b) 120 h back trajectories arriving at 500 m asl at Évora, Portugal.

support the previous mentioned classification in pre-phase and main phase of the desert dust outbreak. Furthermore (Fig. 5b), trajectories arriving at 500 m asl (200 m above ground) never touched the African continent neither in the pre-phase nor during the main phase. This suggests that the transport of mineral particles occur essentially at higher altitudes and vertical mixing as well as gravitational settling processes are responsible for the presence of desert dust particles near surface.

Figure 5 also shows that the particles for this desert dust outbreak travelled from east before arriving in Portugal. The second measurement station at Cabo da Roca is located on the coast nearly 150 km west of Évora at nearly the same geographical latitude. The desert dust plume as observed with sun photometer measurements arrived at the coast slightly more than 4 h later (not shown) than at Évora which corresponds to a mean particle plume speed of less than 40 km h^{-1}. The retrieved columnar particle size distributions and refractive indices were very similar at both stations. Consequently in terms of microphysical particle properties the desert dust plume was homogeneous.

3.2. *Detailed analysis of particle parameters during aircraft over flight*

On 27 May 2006 the aircraft Falcon was flying from the base in Casablanca, Morocco to Portugal and back. The aircraft flew over Évora between 10:30 and 11:00 UTC which coincided closely with the time of the maximum particle concentration at the surface.

3.2.1. Lidar measurements. Figure 6 shows the backscatter ratio (ratio between total and Rayleigh backscattering coefficients) determined from HSR lidar measurements as a west-east cross-section over the Portuguese continent (see Fig. 1 for a map). The layered structures as well as horizontal variations are clearly visible. The data of 2 min (from 10:33 to 10:35 UTC, geographical position indicated in Fig. 1) were averaged to retrieve the vertical profiles of extinction and backscatter coefficient. The ratio of both is the so-called lidar ratio. It is shown in Fig. 7 and

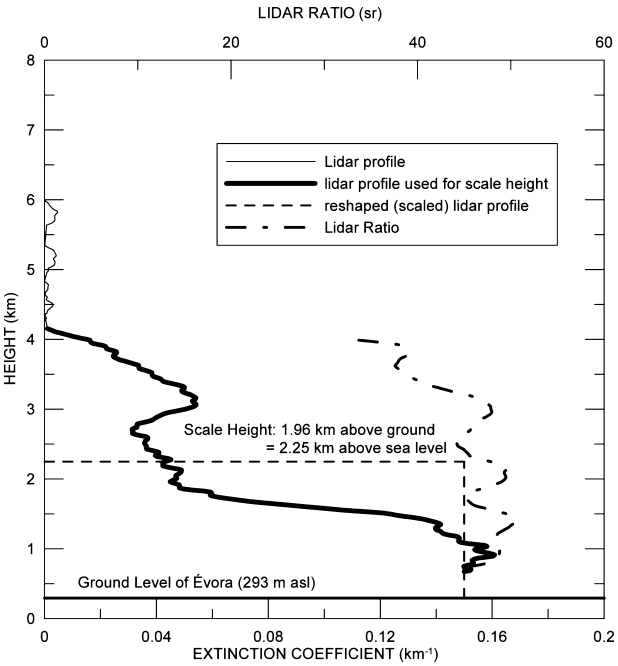

Fig. 7. Vertical profile of the lidar ratio, the extinction coefficient as determined from HSR lidar measurements and the determination of scaling height.

was nearly constant with height with values between 45 and 50 which are typical for desert dust (Esselborn et al., 2008; Tesche et al., 2008). From the altitude independent lidar ratio it can be concluded that the particle type (or mixture) does not change with height. This corresponds with the previous findings based on the analysis of the AE.

Figure 7 shows now the vertical profile of the extinction coefficient averaged over the path corresponding to Fig. 6. The lowest height with valid data does not correspond to the height of the observational platform of CGE. Instead it refers to the highest surface altitude for all profiles included in the average. The figure shows a three-layer structure. From the bottom to

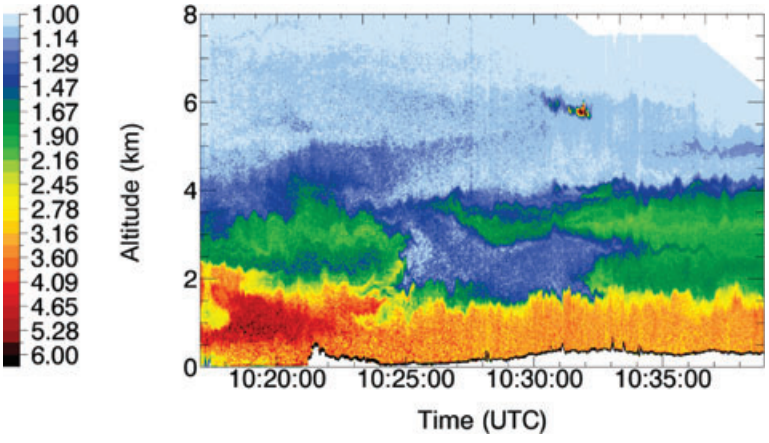

Fig. 6. Backscatter ratio of the parallel polarized laser beam component showing the layering of the particle plume. Data were retrieved from HSR lidar measurements taken between 10:17 and 10:39 UTC along the west-east flight path over Portugal (compare Fig. 1). The airplane passed Cabo da Roca about 10:21 and Évora about 10:33.

about 1.5 km stretches the mixing layer. On top there is an intermediate layer with decreasing extinction coefficient. Finally there is clear distinct particle layer on top between about 2.7 and 4 km. The aircraft took in situ measurements inside the top and intermediate layer.

This profile was rescaled in a way that the extinction coefficient is constant over height and equal to the value at the lowest height of the actual profile. The corresponding layer thickness is 1.96 km and this value is later needed to transform the columnar particle size distribution determined from sun photometry into a volume size distribution.

3.2.2. Aerosol refractive index. From the analysis of the in situ measurements at the aircraft altitude (for details see Petzold et al., 2008) as well as from the inversion of sky brightness measurements using the inversion algorithm by Dubovik and et al. the complex refractive index of the aerosols was derived. The real and imaginary parts are shown separately in Fig. 8 for the two aircraft heights and for the two sun photometer stations (Évora and Cabo da Roca). Because the error in the retrievals of the complex refractive index is unknown, each individual value for the 27 May is included. Therefore, the variability of this quantity is shown which represents in part the uncertainty of the refractive index retrievals. The values derived for the whole column are consistent with the values obtained for the two aircraft heights. This is again (as already concluded from the constant lidar ratio) an indication that the aerosol type does not change significantly with altitude on this day and hence column derived values correspond to in situ derived values. Furthermore, the wavelength-dependent refractive indices for the desert dust aerosol type (consisting of mineral and water-soluble, waso, components), taken from the database OPAC (Hess et al., 1998), are shown.

The spectral behaviours of the refractive indices derived using several methods are different. For the real part of the RI the in situ derived values decrease with wavelengths whereas the column values increase with wavelengths for the same spectral range. On the contrary the imaginary part decreases with wavelength for both retrieval methods. Comparing absolute values and the spectral behaviour with the values from the OPAC database it can be seen that the real part of the refractive indices for the mineral component does not show a spectral dependence and match the measured values. The waso component demonstrates a slight spectral dependence. It is well known and it can be seen that with increasing amount of water the real part of the refractive index tends to lower values. A radio sounding from the Lisbon meteorological weather station at 12 UTC on this day (not shown) indicates that the relative humidity was about 30% near the ground and increased towards the aircraft altitudes to 55% (2380 m) up to 64% (3426 m). Although there is a good match on the real part of the RI, the discrepancies found for the imaginary part do not allow drawing definite conclusions. However, they hint that the desert aerosol particles were still in hydrophobic state.

On the other hand, the imaginary part of the OPAC mineral component is about as twice as high as the measurements but the spectral behaviour is very similar to the measurements. The spectral dependence of the imaginary part for the waso components is very different from the measured one. Therefore, it can be hinted that the waso component plays a negligible role on the complex refractive index of the whole particle population. It will be shown in chapter 3.2.3 below that this is not the case for the size distribution.

3.2.3. Particle size distributions comparisons.. To compare particle size distributions determined using different methods at several altitudes the following corrections were made:

(1) All particle size distributions for different altitudes were corrected to match standard conditions standard temperature and pressure (STP, p_0 is 1013.25 hPa and T_0 is 273.15 K) for a constant volume, i.e. p/T = constant. At the time of the aircraft overpasses (10:49–11:03) the atmospheric thermodynamic conditions were 978.4 hPa and 302.1 K. The respective conditions at the two aircraft altitudes were 277.5 K and 267.8 hPa for 3245 m height and 284.6 K and 783 hPa for 2300 m height.

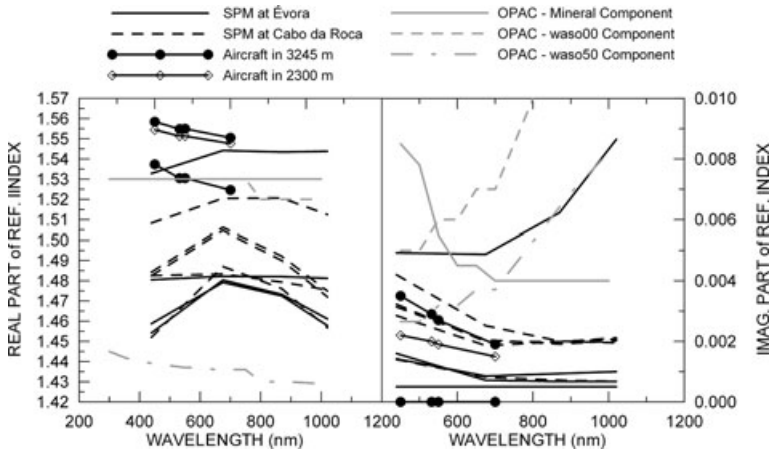

Fig. 8. Real and imaginary parts of the refractive index as derived from in situ measurements in two altitudes and through the inversion of sun photometer measurements at two locations for 27 May 2006 at different measurement times and compared to the OPAC components "mineral" and "water soluble" at 0% (waso00) and 50% (waso50) relative humidity.

(2) Because there was no sun photometer inversion data available during the flight of the aircraft over Évora the following procedure was applied to include the sun photometer derived aerosol size distribution in the comparison.

(a) Averaging of the four available aerosol size distributions obtained from Cimel sun photometer measurements at Évora for 27 May; averaging of the corresponding AODs and calculating the AOD at 532 nm through AE approach. Hereby only particle size distributions retrieved for Évora were used.

(b) Change the aerosol number concentration of the sun photometer derived particle size distribution in such a way that the AOD obtained from the sun photometer measurements matches the lidar integrated AOD. Note that a closure study (Esselborn et al., 2008) was successfully performed for AOD derived from sun photometer and HSR lidar.

(c) Use the scale height (see Fig. 7) to convert columnar (cm^{-2}) into volume aerosol size distribution (cm^{-3}). Hereby the scale height has to be constant for the times of the sun photometer measurements as well as for the times of the lidar measurements. Note that this condition is less strong than demanding identical vertical profiles.

(d) Correct for STP conditions because the sun photometer was operated at the Évora observational platform and not at sea level.

(3) As already mentioned in Section 2, the aerodynamical diameter provided by the APS system was corrected to a geometrical diameter using a density of 2.5 gcm^{-3}.

Figure 9 shows aerosol size distributions for the different measurements and models. It is remarkable that in situ determined aerosol size distribution for the two aircraft heights are nearly identical when transferred to standard conditions and that the aerosol size distribution calculated from sun photometer measurements corresponds quite well in the size range of 0.5–4 μm.

The waso mode from the database OPAC (Hess et al., 1998) can reproduce the small particle mode of the aircraft in situ measurements. The geometrical standard deviation of the waso mode for 50% relative humidity is almost identical to the value for the respective monomodal part of the in situ derived size distribution at the two aircraft heights. As written above, the relative humidity from a radio sounding was 55% at the lower aircraft height (2300 m). For the comparison in Fig. 9, the mode diameter and the geometrical standard deviation of the waso component in OPAC remained unchanged. Only the particle number concentration was adapted.

The comparison with the aerosol size distribution calculated using the LM-MUSCAT model shows that the model reproduces the high particle concentrations at higher elevations over Évora for diameter larger than about 2 μm. For smaller diameters the LM-MUSCAT model results nearly match the ground measurements by the APS. Note that the ground-based in situ derived aerosol size distribution represents a point volume; the aircraft

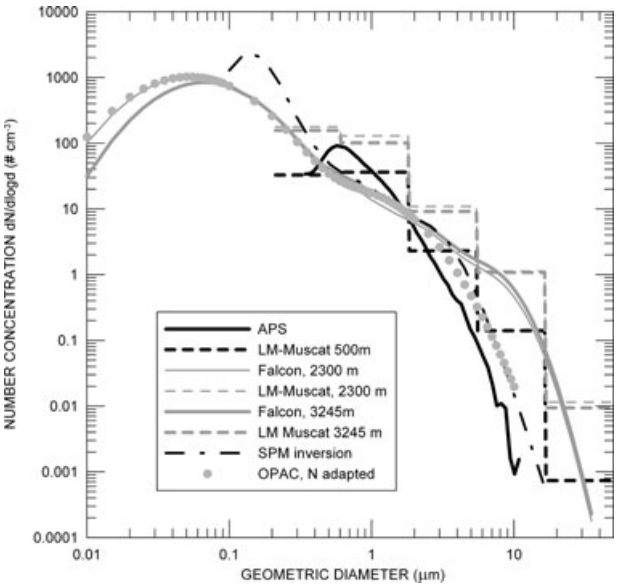

Fig. 9. Comparison of adjusted particle number concentrations from various measurements and models. The legend describes the origin of the data. For the database OPAC the individual aerosol components for the aerosol type desert dust were adapted with their number concentration to match the aircraft in situ measurements for small particles and the aerosol size distribution retrieved from sun photometer measurements for larger particles. The mode diameter as well as the geometric standard deviation remained unchanged.

in situ measured particle size distribution is valid for a horizontal path and the sun photometer derived aerosol size distribution is valid for a vertical column. In contrast the values from the LM-MUSCAT model are representative for a larger volume according to the models horizontal and vertical resolution. The LM-MUSCAT model also overestimates the particle concentration in the accumulation/coarse mode but nearly matches the concentrations for giant particles at the aircraft altitudes.

It is interesting that neither ground-based nor sun photometer retrieved aerosol size distributions contain so many large particles (above 4 μm) in comparison to smaller particles as the particle size distributions retrieved from aircraft measurements. The reasons for this difference are unclear; nevertheless this feature is reproduced by the LM-MUSCAT model and therefore it seems to be related with different air masses and meteorological conditions at the surface and above 2 km height.

4. Summary and conclusion

A desert dust episode lasting several days was investigated using ground-based in situ and remote sensing measurements as well as measurements taken onboard an aircraft. The episode started with a pre-phase on 26 May and the major outbreak reached Évora, Portugal, on 27 May 2006. Close to the time of maximum particle concentration an overpass of the aircraft

Falcon took place over Évora. HSR lidar measurements showed that there was only one aerosol type predominant in the whole column with a corresponding lidar ratio of about 45–50 which is typical for desert dust. The lidar measurements also showed a certain horizontal and vertical variability of aerosol particles. Surface measurements at the time of maximum particle concentrations reached values of about 150 $\mu g\,m^{-3}$ for the particle mass concentration and 130 $M\,m^{-1}$ for the green scattering coefficient. The AOD at 440 nm was as high as 0.53 and the corresponding AE was nearly 0. A comparison between particle size distributions and refractive indices derived from different instruments and models showed in general good agreement but some minor differences could also be observed.

The high frequency of occurrence of such dust outbreaks to continental Portugal and the large uncertainties on their radiative effects emphasize the importance of having multiplatform measurements preferably combined with modelling. Measurements as well as calculations with a particle transport model suggest that there is a relatively higher concentration of very large particles in the upper region of the dust layer than on the surface which is likely connected with meteorological conditions at the observation site (Évora). A higher concentration of larger particles in the free troposphere than near the ground might have implications for the long-wave radiative forcing due to desert dust, because the trapping of thermal radiation depends on the altitude of desert dust.

Furthermore, the use of the measurements of this paper together with the measurements near the source region in Morocco (see various SAMUM papers) enables to link source region and far field together and to investigate altered desert dust properties due to ageing processes during transportation. But this is beyond the scope of this work.

5. Acknowledgments

The project DARPO was funded by the European Commission under the 6th Framework Program within the EUFAR Integrated Infrastructure Initiative. This work was supported by Fundação para a Ciência e Technologia under grants SFRH/BPD/14508/2003, SFRH/BPD/22160/2005, SFRH/BPD/29687/2006 and SFRH/BD/29008/2006 and by the German Research Foundation within the Research Group SAMUM. The authors gratefully acknowledge the NOAA Air Resources Laboratory (ARL) for the provision of the HYSPLIT transport and dispersion model and/or READY website (http://www.arl.noaa.gov/ready.html) used in this publication and they wish to thank Nuno Belo for providing the nephelometer data.

References

Ansmann, A., Bösenberg, J., Chaikovsky, A., Comerón,A., Eckhardt, S. and co-authors. 2003. Long-range transport of Saharan dust to northern Europe: the 11–16 October 2001 outbreak observed with EARLINET. *J. Geophys. Res*. **108**, 4783, doi: 10.1029/2003JD003757.

Anderson, T. L. and Ogren, J. A. 1998. Determining aerosol radiative properties using the TSI 3563 integrating nephelometer. *Aerosol Sci. Technol*. **29**, 57–69.

Borge, R., Lumbreras, J., Vardoulakis, S., Kassomenos, P. and Rodríguez, E. 2007. Analysis of long-range transport influences on urban PM10 using two-stage atmospheric trajectory clusters. *Atmos. Environ*. **41**, 4434–4450.

Cachorro, V. E., Vergaz, R., de Frutos, A. M., Vilaplana, J. M., Henriques, D., and co-authors. 2006. Study of desert dust events over the southwestern Iberian Peninsula in year 2000: two case studies. *Annales Geophysicae* **24**, 1493–1510.

Carlson, T. N. and Benjamin, S. G. 1980. Radiative heating rates for Saharan dust. *J. Atmos. Sci*. **37**, 193–213.

Claquin, T., Schulz, M., Balkanski, Y. and Boucher O. 1998. Uncertainties in assessing radiative forcing by mineral dust. *Tellus* **50B**, 491–505.

Draxler, R. R. and Rolph, G. D. 2003. HYSPLIT (HYbrid Single-Particle Lagrangian Integrated Trajectory) Model access via NOAA ARL READY Website (http://www.arl.noaa.gov/ready/hysplit4.html). NOAA Air Resources Laboratory, Silver Spring, MD.

Dubovik, O. and King M. D. 2000. A flexible inversion algorithm for retrieval of aerosol optical properties from Sun and sky radiance measurements. *J. Geophys. Res*. **105**, 20673–20696.

Dubovik, O., Sinyuk, A., Lapyonok, T., Holben, B. N., Mishchenko, M. and co-authors. 2006. Application of light scattering by spheroids for accounting for particle non-sphericity in remote sensing of desert dust. *J. Geophys. Res*. **111**, D11208, doi: 10.1029/2005JD006619.

Eck, T. F., Holben, B. N., Reid, J. S., Dubovik, O., Smirnov, A. and co-authors. 1999. Wavelength dependence of the optical depth of biomass burning, urban, and desert dust aerosols. *J. Geophys. Res*. **104**, 31 333–31 349.

Elias, T., Silva, A. M., Belo, N., Pereira, S., Formenti, P. and co-authors. 2006. Aerosol extinction in a remote continental region of the Iberian Peninsula during summer. *J. Geophys. Res*, **111**, D14204, doi: 10.1029/2005JD006610.

Esselborn, M., Wirth, M., Fix, A., Tesche, M. and Ehret, G. 2008. Airborne high spectral resolution lidar for measuring aerosol extinction and backscatter coefficients. *Appl. Opt*. **47**, 346–358.

Esselborn, M., Wirth, M., Fix, A., Weinzierl, B., Rasp, K. and co-authors. 2008. Spatial distribution and optical properties of Saharan dust observed by airborne high spectral resolution lidar during SAMUM 2006, *Tellus* **61B**, doi: 10.1111/j.1600-0889.2008.00394.x.

Fiebig, M., Stein, C., Schröder, F. Feldpausch, P. and A. Petzold 2005. Inversion of data containing information on the aerosol particle size distribution usingmultiple instruments. *J. Aerosol Sci*. **36**, 1353–1372.

Fletcher, B. 1976. The incipient motion of granular materials. *J. Phys. D: Appl. Phys*. **9**, 2471–2478.

Fratini, G., Ciccioli, P., Febo, A., Forgione, A. and Valentini, R. 2007. Size-segregated fluxes of mineral dust from a desert area of northern China by eddy covariance, *Atmos. Chem. Phys.* **7**, 2839–2854.

Hand, J. L. and Malm, W. C. 2007. Review of aerosol mass scattering efficiencies from ground-based measurements since 1990. *J. Geophys. Res.* **112**, D16203, doi: 10.1029/2007JD008484.

Haywood, J.M., Francis, P. N., Geogdzhayev, I., Mishchenko, M. and Frey, R. 2001. Comparison of Saharan dust aerosol optical depths

retrieved using aircraft mounted pyranometers and 2-channel AVHRR algorithms, *Geophys. Res. Lett.* **28**, 2393–2396.

Heinold, B., Helmert, J., Hellmuth, O., Wolke, R., Ansmann, A. and co-authors. 2007. Regional modeling of Saharan dust events using LM-MUSCAT: model description and case studies, *J. Geophys. Res.* **112**, D11204, doi: 10.1029/2006JD007443.

Heinold, B., Tegen, I., Knippertz, P., Laurent, B., Schepanski, K. and co-authors. 2008. Regional Saharan dust modelling during the SAMUM 2006 campaign. *Tellus* **61B**, doi: 10.1111/j.1600-0889.2008.00387.x.

Hess, M., Koepke, P. and Schult, I. 1998. Optical properties of aerosols and clouds: the software package OPAC. *Bull. Am. Meteorol. Soc*. **79**, 831–844.

Hinds, W.C. 1999. *Aerosol Technology: Properties, behaviour, and Measurements of Airborne Particles* 2nd Edition. John Wiley & Sons, New York, 483 pp.

Holben, B. N., Eck, T. F., Slutsker, I., Tanré, D. Buis, J. P. and co-authors. 1998. AERONET—a federated instrument network and data archive for aerosol characterization. *Remote Sens. Environ*. **66**, 1–16.

Ishizaka, Y. and Ono, A. 1982. Mass-size distribution of the principal minerals of yellow sand dust in the air over Japan, *Idojaras* **86**, 249–253.

Iwasaka, Y., Shi, G.-Y. Shen, Z., Kim, S., Trochkin, D., and co-authors. 2003. Nature of atmospheric aerosols over the desert area in the Asian continent: chemical state and number concentration of particles measured at Dunhuang, China. *Water, Air Soil Pollut.: Focus* **3**, 129–145.

Pereira, S.N. 2006. *Utilization of a Particle Monitor for the Determination of the Aerosol Mass Concentration at the Surface and Validation of the Measurements (in Portuguese)*, Master thesis. University of Évora, Portugal, 90 pp.

Pereira, S., Wagner, F. and Silva, A.M. 2008. PM10 air quality assessment at a Portuguese rural city using a TEOM instrument. In: *Proceedings of European Aerosol Conference 9–14 September 2007*, Salzburg, Austria.

Pérez, C., Nickovic, S., Baldasano, J. M., Sicard, M., Rocadenbosch, F. and co-authors. 2006. A long Saharan dust event over the western Mediterranean: Lidar, Sun photometer observations, and regional dust modeling. *J. Geophys Res*. **111**, D15214, doi: 10.1029/2005JD006579.

Petzold, A., Rasp, K., Weinzierl, B., Esselborn, M., Hamburger, T. and co-authors. 2008. Saharan dust absorption and refractive index from aircraft-based observations during SAMUM 2006. *Tellus* **61B**, doi: 10.1111/j.1600-0889.2008.00383.x.

Prospero, J.M. 1999. Long-term measurements of the transport of African mineral dust to the southeastern United States: implications for regional air quality. *J. Geophys. Res.* **104**, 15 917–15 927.

Redelsperger, J.-L., Thorncroft, C. D., Diedhiou, A., Lebel, T., Parker, D. J. and co-authors. 2006. African monsoon multidisciplinary analysis: an international research project and field campaign. *Bull. Am. Meteorol. Soc*. **87**, 1739–1746.

Reid, J.S., Kinney, J. E., Westphal, D. L., Holben, B. N., Welton, E. J., and co-authors. 2003. Analysis of measurements of Saharan dust by airborne and groundbased remote sensing methods during the Puerto Rico Dust Experiment (PRIDE). *J. Geophys. Res*. **108**, 8586, doi: 10.1029/2002JD002493.

Rodríguez, S., Querol, X., Alastuey, A., Kallos, G. and Kakaliagou, O. 2001. Saharan dust contribution to PM10 and TSP levels in Southern and eastern Spain. *Atmos. Environ*. **35**, 2433–2447.

Rolph, G.D. 2003. *Real-time Environmental Applications and Display sYstem (READY)*. NOAA Air Resources Laboratory, Silver Spring, MD . Available at: http://www.arl.noaa.gov/ready/hysplit4.html.

Russell, P.B. and Heintzenberg, J. 2000. An overview of the ACE-2 clear sky column closure experiment (Clearcolumn). *Tellus* **52B**, 463–483.

Shen, Y., Shen, Z., Du, M. and Wang, W. 2005. Dust emission over different land surface in the arid region of northwest China. *J. Meteorol. Soc. Jpn.* **83**, 935–942.

Smirnov, A., Holben, B. N., Eck, T. F., Dubovik, O. and Slutsker, I. 2000. Cloud-screening and quality control algorithms for the AERONET database. *Remote Sens. Environ*. **73**, 337–349.

Tanré, D., Haywood, J., Pelon, J., Léon, J.F., Chatenet, B. and co-authors. 2003. Measurement and modeling of the Saharan dust radiative impact: overview of the Saharan Dust Experiment (SHADE). *J. Geophys. Res*. **108**, 8574, doi: 10.1029/2002JD003273.

Tegen, I., Harrison, S. P., Kohfeld, K., Prentice, I. C., Coe, M. and co-authors. 2002. Impact of vegetation and preferential source areas on global dust aerosol: results from a model study. *J. Geophys. Res*. **107**, 4576, doi: 10.1029/2001JD000963.

Tesche, M., Ansmann, A., Müller, D., Althausen, D., Heese, B. and co-authors. 2008. Vertical profiling of Saharan dust with Raman lidars and airborne HSRL in southern Morocco during SAMUM. *Tellus* **61B**, doi: 10.1111/j.1600-0889.2008.00390.x.

Washington, R., Todd, M., Middleton, N. J. and Goudie, A.S. 2003. Dust-storm source areas determined by the total ozone monitoring spectrometer and surface observations. *Ann. Assoc. Am. Geogr*. **93**, 297–313.

Weinzierl, B., Petzold, A., Esselborn, M., Wirth, M. and co-authors. 2008. Airborne measurements of dust layer properties, particle size distribution and mixing state of Saharan dust during SAMUM 2006. *Tellus* **61B**, doi: 10.1111/j.1600-0889.2008.00392.x.

Winfield, K.A. .2000. Factors controlling water retention of alluvial deposits. *Western Mojave Desert*, available at http://wwwrcamnl.wr.usgs.gov/uzf/winfield.thesis.pdf.